BJR

Received: 10 June 2014 | Revised: 16 November 2014 | Accepted: 19 November 2014

doi: 10.1259/bjr.20140412

Cite this article as:
Abramyuk A, Hietschold V, Appold S, von Kummer R, Abolmaali N. Radiochemotherapy-induced changes of tumour vascularity and blood supply estimated by dynamic contrast-enhanced CT and fractal analysis in malignant head and neck tumours. Br J Radiol 2015;88:20140412.

FULL PAPER

Radiochemotherapy-induced changes of tumour vascularity and blood supply estimated by dynamic contrast-enhanced CT and fractal analysis in malignant head and neck tumours

[1]A ABRAMYUK, MD, [2]V HIETSCHOLD, PhD, [3]S APPOLD, MD, [1]R VON KUMMER, MD and [4]N ABOLMAALI, MD

[1]Department of Neuroradiology, Medical Faculty and University Hospital Carl Gustav Carus, TU Dresden, Germany
[2]Institute and Policlinic of Diagnostic Radiology, Medical Faculty and University Hospital Carl Gustav Carus, Dresden, Germany
[3]Department of Radiation Oncology, Medical Faculty and University Hospital Carl Gustav Carus, Dresden, Germany
[4]Department of Radiology, Medical Faculty and University Hospital Dresden-Friedrichstadt, Dresden, Germany

Address correspondence to: Dr Andrij Abramyuk
E-mail: *Andrij.Abramyuk@uniklinikum-dresden.de*

Objective: To investigate radiochemotherapy (RChT)-induced changes of transfer coefficient (K^{trans}) and relative tumour blood volume (rTBV) estimated by dynamic contrast-enhanced CT (DCE-CT) and fractal analysis in head and neck tumours (HNTs).
Methods: DCE-CT was performed in 15 patients with inoperable HNTs before RChT, and after 2 and 5 weeks. The dynamics of K^{trans} and rTBV as well as lacunarity, slope of log(lacunarity) *vs* log(box size), and fractal dimension were compared with tumour behaviour during RChT and in the 24-month follow-up.
Results: In 11 patients, an increase of K^{trans} and/or rTBV after 20 Gy followed by a decrease of both parameters after 50 Gy was noted. Except for one local recurrence, no tumour residue was found during the follow-up. In three patients with partial tumour reduction during RChT, a decrease of K^{trans} accompanied by an increase in rTBV between 20 and 50 Gy was detected. In one patient with continuous elevation of both parameters, tumour progressed after RChT. Pre-treatment difference in intratumoral heterogeneity with its decline under RChT for the responders *vs* non-responders was observed.
Conclusion: Initial growth of K^{trans} and/or rTBV followed by further reduction of both parameters along with the decline of the slope of log(lacunarity) *vs* log(box size) was associated with positive radiochemotherapeutic response. Increase of K^{trans} and/or rTBV under RChT indicated a poor outcome.
Advances in knowledge: The modification of K^{trans} and rTBV as measured by DCE-CT may be applied for the assessment of tumour sensitivity to chose RChT regimen and, consequently, to reveal clinical impact allowing individualization of RChT strategy in patients with HNT.

Combined radiochemotherapy (RChT) plays an important role in the management of malignant head and neck tumours (HNTs) and has been considered as the standard treatment for clinically non-operable cases.[1] Experimental observations indicate that RChT, besides direct cytotoxic effect, exerts its influence also on tumorangiogenesis.[2–4] Folkman and Camphausen[5] suggested that endothelial cells may represent the principal targets for irradiation. Some studies reported the upregulation of angiogenic pathways and activation of different growth factors during radiotherapy as a kind of tumour response to radiation stress.[2,3,6,7] By affecting endothelial cells in the tumour's vascular bed, chemotherapeutic agents indirectly modify neovascularization and blood supply, thus modulating tumour radiosensitivity.[4,8,9]

At the same time, malignant tumours display substantial internal heterogeneity in cellular morphology, vascularization and metabolism.[10–12] Intrinsic pattern of microenvironment and blood supply is among factors that are influencing the efficacy of RChT in every individual tumour.[13–15]

Therefore, implementation of advanced imaging techniques into clinical routine may provide morphological and functional information that may help characterizing tumour biology. Tumours with certain biological features, potentially resistant to standard treatment regimens, could then be treated with other measures, improving the chances of success.[16]

Dynamic contrast-enhanced CT (DCE-CT) is an evolving functional imaging method assessing vascularity and blood supply in normal organs or in tumour tissue.[17]

This work aimed to clarify the clinical relevance of DCE-CT in patients with HNT. We hypothesized that transfer coefficient (K^{trans}) and relative tumour blood volume (rTBV) as well as their intratumoral heterogeneity are additional functional parameters associated with RChT outcome. To prove this, the dynamics of K^{trans} and rTBV as well as lacunarity, slope of log(lacunarity) *vs* log(box size), and fractal dimension was estimated by DCE-CT and fractal analysis. The influence of tumour shape and size on lacunarity parameters thereby was reduced by modification of the gliding box counting method.

METHODS AND MATERIALS

Patients

We prospectively enrolled 15 consecutive patients (median age, 51 years; range, 47–74 years) with histologically proven, clinically inoperable oropharyngeal or hypopharyngeal squamous cell carcinoma (stages T3N0M0—T4N2cM0) into this study. Details of the patient's cohort have been published previously.[18] Further inclusion criteria comprised no previous therapy (chemotherapy, surgery), no metal teeth implants causing beam-hardening artefacts and follow-up time of 24 months in surviving patients ($n = 12$) or till last visit before death ($n = 3$). Clinical follow up included physical status observations, routine radiology examination including abdominal ultrasound, whole-body fluorine-18 fludeoxyglucose (FDG) positron emission tomography (PET)/CT and/or MRI of the neck as well as laboratory tests and survival history. The study protocol was approved by the institutional review board of Medical Faculty and University Hospital Carl Gustav Carus, Dresden, Germany. All patients gave written informed consent. Determination of responder/non-responder was based on CT data using World Health Organization criteria.[19]

Treatment

All patients were treated with radiotherapy with curative intention. Simultaneously, all these patients received chemotherapy that consisted of intravenous infusion of cisplatin ($30\,mg\,m^{-2}$ per week) during the 6 weeks of radiotherapy and 5-fluorouracil ($600\,mg\,m^{-2}$ per day) during Days 1–5 of the first week only. After treatment, all patients were divided into responders group (no residual tumour was seen after completing the RChT) and non-responders group (partial tumour regression or progression under the RChT).

Imaging

DCE-CT was performed before RChT, and after 2 weeks (20 Gy for two cycles cisplatin + one cycle 5-fluorouracil) and 5 weeks (50 Gy for five cycles cisplatin + one cycle 5-fluorouracil) of RChT using PET/CT scanner (Biograph 16; Siemens Healthcare Sector, Knoxville, TE). The patients were placed in treatment position on a flat-top couch mounted to the conventional curved diagnostic couch of the PET/CT scanner. Positioning of patients was carried out with lateral and sagittal lasers. Specific head immobilization device attached to the flat-top couch was used to exactly reproduce positioning as during radiotherapy. For quantitative evaluation of blood supply, we used X-ray CT. In contrast to dynamic MRI, here the change of Hounsfield unit values is proportional to the amount of contrast medium in a voxel. So, for the concept of this study, a more robust and therefore reliable measurement strategy was evaluated as more important than the avoidance of an additional radiation exposure, which is small compared with the therapy dose.

As previously published[18] plain CT was performed through the tumour to receive baseline data for further blood supply parameter measurements. Thereafter, DCE-CT was acquired through the same region following intravenous administration of contrast agent ($4\,ml\,s^{-1}$, 100 ml of Ultravist® 370; Bayer Schering Pharma AG, Berlin, Germany) with saline flushing using a double head power injector (Injectron CT 2, Medtron, Saarbrücken, Germany) through an 18-G antecubital cannula. Patients were warned to avoid taking deep breaths when experiencing a "hot flush" owing to rapid bolus injection of iodinated contrast agent. Images were acquired during shallow respiration. The following scanning parameters were used: 120 kV; 150 mAs; rotation time, 0.5 s; reconstruction width, 1.5 mm; and field of view, 250 mm. 30 images were collected continuously over 60 s (1 image per 2 s).

Image analysis

Acquired data were transferred to a Syngo Multimodality Workplace (Siemens Healthcare Sector, Erlangen, Germany) for analysis. The K^{trans} and rTBV were estimated by modified Patlak analysis using pixel-based software (VPCT; Siemens Healthcare Sector) yielding colour-coded maps of spatial distribution of these parameters. The input function required for modelling of temporal contrast agent distribution was derived from external carotid artery in all cases. The K^{trans} represents passage of contrast agent between the blood and the extravascular extracellular space and is cumulatively affected by both flow and permeability surface area product.[20,21] The rTBV is a quantitative measure for the volume percentage of capillary blood in a voxel filled with tumour tissue.

Intratumoral blood supply heterogeneity was determined from DCE-CT data by means of lacunarity, slope of log(lacunarity) *vs* log(box size), and fractal dimension using fractal analysis. For evaluation of lacunarity, parameter maps were processed with an in-house program written in IDL (Exelis Visual Information Solutions, Inc., Boulder, Co).

Lacunarity is a measure of structural heterogeneity (non-uniformity) or degree of structural variance within an object depending on neighbourhood size.[22,23] Higher lacunarity values indicate higher structural heterogeneity, that is, more non-uniformity of structures within an image. The slope of log(lacunarity) *vs* log(box size) describes the degree to which the heterogeneity pattern looks like a fractal structure. For a clear fractal image, this slope should be equal to zero. Negative values indicate a more uniform characteristic for larger structures. The fractal dimension is a measure of the complexity of a fractal structure (for instance, linear structures have a fractal index of one, squares one of two, the Sierpinski's triangle is described with a fractal index of about 1.585). We applied the definition used in Goh et al.[24]

To make precise differentiation between tumour and normal neck tissues, regions of interest (ROIs) at the primary tumour site were visually determined from combined FDG-PET/CT images and subsequently transferred manually to DCE-CT data sets for analysis. ROI delineation as well as quantitative estimation of K^{trans} and rTBV was carried out by an experienced professional (radiological experience of more than 15 years). First, K^{trans} and rTBV maps were masked to show tumour data only using ROIs on CT images. Thereafter, masked K^{trans} and rTBV maps were binarized using median local adaptive thresholding with a 13×13 pixel neighbourhood. Finally, mean lacunarity, the slope of log(lacunarity) *vs* log(box size) and fractal dimension were evaluated from binarized parameter maps by means of a gliding box counting method setting the pixel to one if the pixel value x is in a certain range r around the median m in the neighbourhood ($m - r \leq x \leq m + r$) and to zero otherwise. Considering the limited size of tumour areas in calculation of lacunarity parameters, we normalized the sum of marked pixels in the binary image contained in the gliding box (the so-called "mass") to the number of pixels in the box that belong to the tumour ROI. This way, we avoided contributions to the lacunarity, which in fact are caused by the outer shape of the tumour. For the fractal dimension, we applied the definition used in Goh et al.[24]

Statistics

A statistical analysis was performed using Microsoft Excel® (Microsoft, Redmond, WA). For both K^{trans} and rTBV, we used the Wilcoxon test for univariate group comparisons between the values befor RChT, and after 20 Gy and 50 Gy. This test checks for significantly different numbers of positive and negative pair differences. Therefore, it is sensitive for significant changes of the median values during the course of RChT. Mean values were tested for significant difference by means of the Welch modification of the *t*-test for samples with unknown, possible different variances. The *p*-values of ≤ 0.05 were considered to be statistically significant. As a simple inhomogeneity parameter, we calculated the half difference between the 84.2% and 15.8% percentiles (percentile difference). For gaussian-distributed values, this parameter is equal to the standard deviation. In addition, on a qualitative base, we tried to find characteristic patterns of changes in K^{trans} and rTBV during RChT for the end points "complete tumour regression at the end of RChT", "partial tumour regression at the end of RChT", "local tumour progression" and "patient died" in the 24-month follow-up.

RESULTS

We observed two different patterns of K^{trans} and rTBV dynamics during RChT associated with tumour response and patient survival. Clinically, the appropriate groups are characterized by the following behaviour: responders: 11 patients with complete tumour regression to the end of RChT [1 patient with local tumour progression after the end of this study (follow-up after 12 months) belongs to the responder group as well]; non responders: 4 patients with no (1 patient) or partial tumour regression only (3 patients), 2 of them died within the 12-month follow-up period. The characteristics of K^{trans} and rTBV dynamics are illustrated in Figure 1 and Tables 1 and 2. In the responders group, an increase of K^{trans} and/or rTBV after 20 Gy was followed by a decline of both parameters after 50 Gy ($p < 0.05$). A steeper rising and sloping of K^{trans} and rTBV under RChT correlated with more distinct morphological tumour regression in four patients. By contrast, in one patient with continuous elevation of both K^{trans} and rTBV under RChT, no response during treatment and severe tumour progression in the first 6 months of follow-up was observed.

In another three non-responders, a slight decrease of K^{trans} under RChT accompanied by a marked increase of rTBV between 20 and 50 Gy was detected. Concerning the homogeneity parameters derived from both K^{trans} and rTBV parameter images, at the beginning of the therapy, we observed a significant difference of the slopes of log(lacunarity) *vs* log(box size) for the responders *vs* non-responders group mean values ($p < 0.05$). The steeper negative slope in the non-responders group indicates larger dependence of the inhomogeneity on the structure size. Subsequent decrease of the absolute value of this slope was revealed during RChT in both groups. The fractal dimension of the rTBV images tends to decrease for the responders and to increase for the non-responders. Figure 1 presents dynamics of K^{trans} and rTBV during RChT. Corresponding images are shown in Figure 2. The significance matrix for the parameter changes between the therapy steps mentioned above is shown in Table 1.

No correlation was found between any of these parameters and tumour behaviour in the 24-month follow-up. A high correlation between the percentile difference and the lacunarity of the parameter images of K^{trans} was noted (correlation coefficient, 0.78). For that of rTBV, for the lacunarity of rTBV, it was less pronounced (correlation coefficient, 0.48).

DISCUSSION

We used DCE-CT and fractal analysis to study RChT-induced changes of vascularity in HNTs. We are not aware of similar studies investigating modifications of intratumoral vascularity and blood supply heterogeneity in HNTs under RChT. In the responders group, we found a growth of K^{trans} and/or rTBV during the first 2 weeks of treatment (20 Gy), followed by a continuous decrease of both parameters during the following 3 weeks of treatment (50 Gy). Quite similarly, Cao et al[25] investigating the effect of radiation therapy on the blood–brain barrier permeability of primary brain tumours using dynamic-enhanced MRI noted a gradual decrease of K^{trans} as soon as 1 month after the treatment. More recently, Almeida-Freitas et al[26] reported a significant reduction in K^{trans} values of cerebral metastasis 4–8 weeks after stereotactic radiosurgery. An increase of one or both parameters at the beginning of treatment should not be misinterpreted as increasing resistance. It may be indicative of an increased extracellular space in tumours exhibiting progressively permeable vessel walls or an increasing number of tumour microvessels, which may result in increased radiosensitivity and better local control, as presented before.[27,28] This hypothesis could be tested by application of the Tofts model for example. During the second period of treatment (3–5 weeks), a cytotoxic effect of irradiation together with cisplatin may have manifested itself on endothelial cells of vessels, which may have led to thrombosis and occlusion of small vessels. Additionally, changes of these parameters after 20 and 50 Gy, respectively, might be affected by an initial increase of blood supply owing to

Figure 1. (a) Dynamics of transfer coefficient (K^{trans}) and relative tumour blood volume (rTBV) during radiochemotherapy (RChT) in the responders group. (b) Dynamics of K^{trans} and rTBV during RChT in patients showing morphologically partial response or local tumour progress (non-responders group).

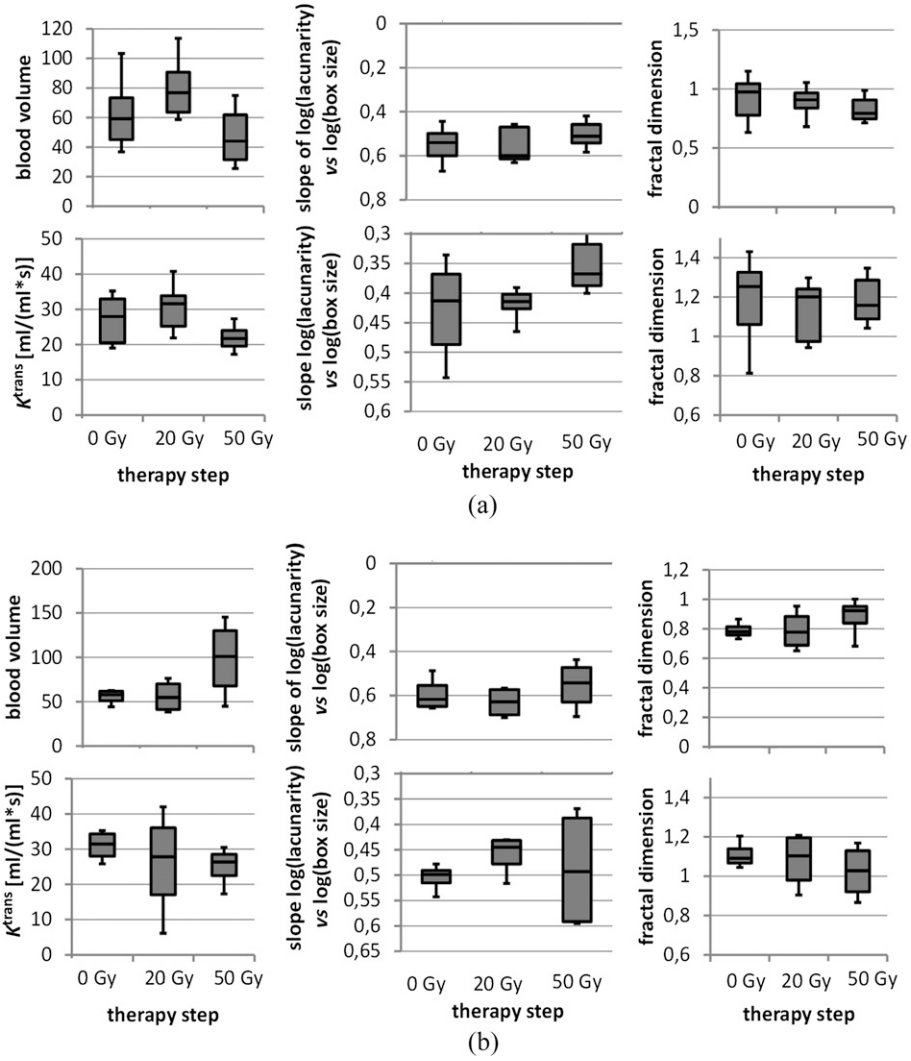

the loss of overall tumour cell volume, followed by its decrease overcompensating this initial effect as a result of occlusion and/or destruction of tumour vessels. This is in good agreement with a tendency to decrease tumour blood volume after 50 Gy in the partial responders group in contrast to further increasing rTBV in the non-responders. Established individual variations of K^{trans} and rTBV during the treatment indicate, however, that pathomorphological mechanisms of RChT-induced changes of tumour vascularity and blood supply as well as their impact on outcome are not fully understood. The outlier in our "responders" group underlines this. On the basis of the accepted models of tumour pathophysiology, the drop of K^{trans} between 20 and 50 Gy in the non-responders group is not completely comprehensible. It may be explained through the fact that under flow-limited conditions, K^{trans} equals the blood plasma flow per unit volume of tissue.[20] Therefore, if tumour supplying smaller arteries would be affected by the therapy, K^{trans} could be reduced owing to decreased blood flow even if number and size of the capillaries (and thus the rTBV) were not (or not yet) changed. In agreement with the earlier published data,[29,30] local tumour progress was diagnosed during follow-up in a patient showing an elevation of both K^{trans} and rTBV under RChT. This event could be explained by the hypothesis that ionizing irradiation may in some instances provoke undesired effects through the induction of the vascular endothelial growth factor and its receptors in residual tumour cells, which is a powerful antiapoptotic factor for endothelial cells.[15] Failure of chemotherapy to compensate these undesired effects may lead to local tumour relapse.[30–32]

Tumour tissues easily become hypoxic and necrotic because of altered vascular architecture, rapid proliferation and insufficient blood supply.[6] As published before,[33] intratumoral heterogeneity correlates well with the morphological response to the therapy, at which tumours with higher internal heterogeneity show poorer prognosis. In our study, already prior to the therapy, significant differences between responders and non-responders were seen concerning heterogeneity properties. In addition, a reduction of "structured heterogeneity" was already observed

Table 1. Significance matrix for parameter changes during radiochemotherapy

Radiation dose (Gy)	Blood volume (%)	Slope blood volume (%)	Fractal dimension blood volume (%)	K^{trans} (%)	Slope K^{trans} (%)	Fractal dimension K^{trans} (%)
Responders						
0 *vs* 20	3.5	9.4	12.9	11.0	9.4	6.5
0 *vs* 50	0.7	2.7	6.5	0.4	1.7	5.3
20 *vs* 50	0.3	4.0	2.3	0.3	0.9	19.5
Non-responders						
0 *vs* 20	25.0	3.6	25.0	11.6	1.7	11.6
0 *vs* 50	3.6	17.9	6.8	11.6	11.6	3.6
20 *vs* 50	3.6	11.6	11.6	25.0	17.9	1.7

K^{trans}, transfer coefficient.
Slope, slope of log(lacunarity) *vs* log(box size).
p-values from the Wilcoxon test for asymmetric distribution of pair differences are shown. Significant changes are highlighted in grey.

after 20 Gy and was continued at 50 Gy for both K^{trans} and rTBV. These changes were seen in the lacunarity itself (although not significant) as well as in the slope of log(lacunarity) *vs* log(box size) ($p < 0.05$). Lacunarity and the width of the distribution of parameters such as K^{trans} or rTBV resp. both describe aspects of inhomogeneity of the tissue region under investigation. Nevertheless, the easy-to-calculate difference between the 84.2% and 15.8% percentiles was not suitable as a surrogate parameter for lacunarity measure. The continuous decline of their absolute values could be interpreted as a reduction of structures of more or less defined size. A higher fractal dimension indicates more complex shapes forming the heterogeneity of the tumours—hypothetically, for instance, owing to heterogeneous neovascularization. In agreement with the measurements by Goh et al[24] in the case of colorectal tumours, a higher fractal dimension therefore might give evidence for higher malignancy with higher probability for cell division resulting in higher radiosensitivity and/or better response to chemotherapy. This hypothesis is in agreement with the fractal dimensions measured in the K^{trans} as well as rTBV parametric images. For rTBV, such possible tendency was even less pronounced and also not significant—so five of the six pairs of fractal dimensions are in agreement with this hypothesis. The apparent deviation of the rTBV fractal dimension after 50 Gy is non-significant (two-sided *t*-test assuming equal variances: $p = 19.2\%$ and assuming non-equal variances: $p = 5.2\%$). At a glance, therapy effects can be demonstrated by means of the structural parameters from fractal analysis. But its clinical value in HNTs still remains questionable. Some works[18,34,35] showed that parameters are useful in outcome prediction. However, in this study, no significant correlation between pre-therapeutic values of K^{trans} or rTBV and outcome was found, which is in agreement with earlier reports on other tumour entities.[11,12] It may be postulated that these parameters have prognostic value only in certain limits. Pronounced heterogeneity of intratumoral microcirculatory milieu, the existence of heterogeneous hypoxic regions, makes it difficult to predict tumour response to treatment in a particular case.[36] Another reason for these discrepancies might be the differences in treatment regimens and the observed end points.[30]

Table 2. Median values from Figure 1

Radiation dose (Gy)	Blood volume	Slope blood volume	Fractal dimension blood volume	K^{trans}	Slope K^{trans}	Fractal dimension K^{trans}
Responders						
0	59.30	−0.54	0.98	27.94	−0.41	1.25
20	76.76	−0.60	0.91	31.62	−0.41	1.20
50	44.00	−0.51	0.79	21.71	−0.37	1.16
Non-responder						
0	57.86	−0.62	0.78	31.49	−0.50	1.09
20	54.79	−0.63	0.78	27.83	−0.45	1.10
50	100.90	−0.54	0.92	26.37	−0.49	1.03

K^{trans}, transfer coefficient.

Figure 2. (a) Dynamic contrast-enhanced CT (DCE-CT) colour-coded maps of relative tumour blood volume (rTVB) and transfer coefficient (K^{trans}) before radiochemotherapy (RChT), and after 20 Gy and 50 Gy (responders group). (b) DCE-CT colour-coded maps of rTVB and K^{trans} before RChT, and after 20 Gy and 50 Gy (non-responders group).

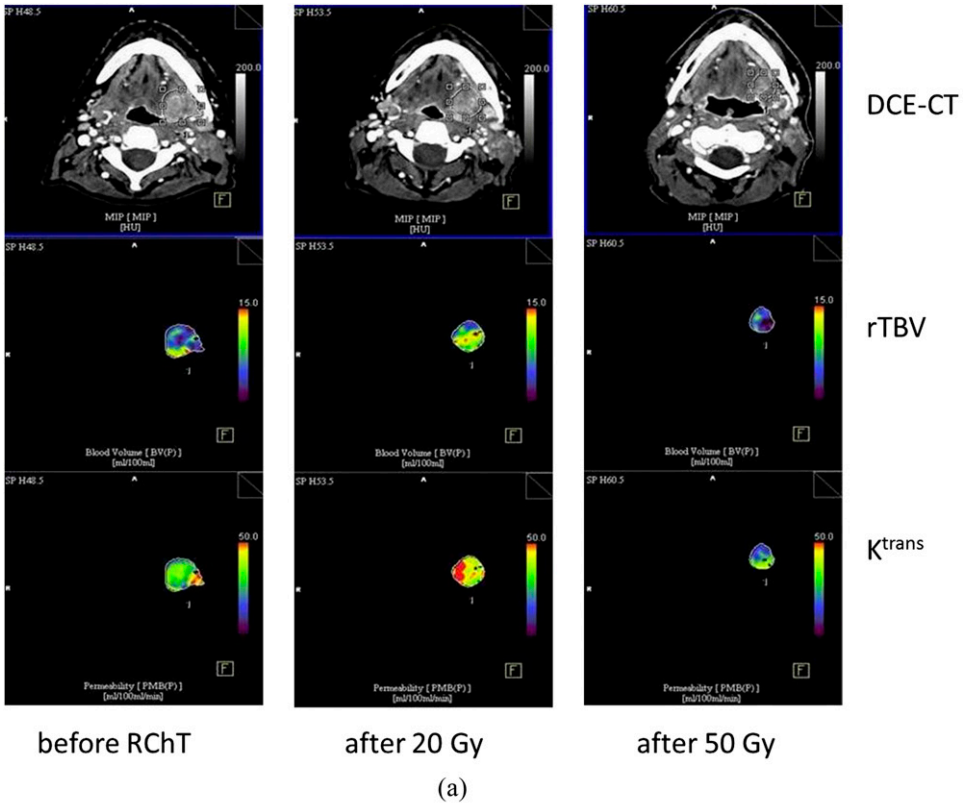

(a)

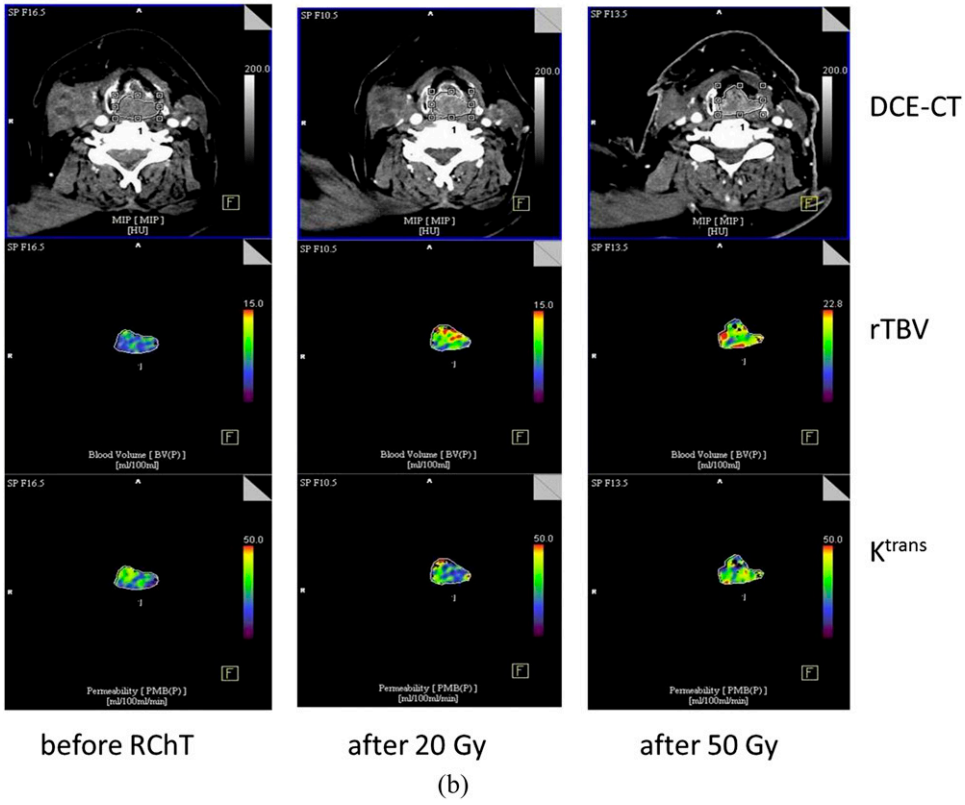

(b)

We acknowledge some limitations of our study. As in other imaging studies including HNT patients, swallowing-related tumour movement and artefacts caused by injection of high concentrations of iodine contrast agent may deteriorate DCE-CT data acquisition and analysis. The input function required for modelling of temporal contrast agent distribution was derived from external carotid artery in all cases. The comparatively small diameter of this vessel generates potential sampling errors propagating into final analysis. The small size of tumours at least in one direction (*e.g.* small rim of active tumour around a larger necrotic area, especially after 20 and 50 Gy) is an essential source of errors in fractal analysis. In this article, efforts have been made to consider the influence of the tumour boundaries on the fractal parameters by allowing for boxes that contain only partial tumour tissue and performing appropriate normalization of their weight. Finally, the relative small number of patients prohibits definitive conclusions.

Nevertheless, our results can be corroborated in prospective randomized studies to prove their relevance for clinical practice.

CONCLUSION

Initial growth of K^{trans} and/or rTBV followed by the reduction of both parameters to the end of treatment along with the decline of the slope of log(lacunarity) *vs* log(box size) was found to be associated with positive radiochemotherapeutic response. Continuous increase of K^{trans} and/or rTBV under RChT indicated a poor outcome. K^{trans} and rTBV as well as intratumoral heterogeneity parameters based on these parameters measured by DCE-CT may be applied for the assessment of tumour sensitivity to chose RChT regimen and, consequently, to reveal clinical impact allowing individualization of RChT strategy in patients with HNT.

FUNDING

This research was supported by the Federal Ministry of Education and Research, Germany (BMBF contract 03ZIK042).

ACKNOWLEDGMENTS

We thank Gabriele Kotzerke, Kathrin Gericke and Arne Koch for the invaluable assistance in selection and radiological imaging of the cohort.

REFERENCES

1. Pazdur R, Coia L, Hoskins W, Wagman L, eds. *Cancer management: a multidisciplinary approach*. 9th edn. New York, NY: CMP Healthcare Media; 2005.
2. Gorski DH, Beckett MA, Jaskowiak NT, Calvin DP, Mauceri HJ, Salloum RM, et al. Blockage of the vascular endothelial growth factor stress response increases the antitumor effects of ionizing radiation. *Cancer Res* 1999; **59**: 3374–8.
3. Koukourakis MI, Giatromanolaki A, Sivridis E, Simopoulos K, Pissakas G, Gatter KC, et al. Squamous cell head and neck cancer: evidence of angiogenic regeneration during radiotherapy. *Anticancer Res* 2001; **21**: 4301–9.
4. Albertsson P, Lennernäs B, Norrby K. Chemotherapy and antiangiogenesis: drug-specific effects on microvessel sprouting. *Apmis* 2003; **111**: 995–1003.
5. Folkman J, Camphausen K. Cancer. What does radiotherapy do to endothelial cells? *Science* 2001; **293**: 227–8.
6. Furuya M, Nishiyama M, Kasuya Y, Kimura S, Ishikura H. Pathophysiology of tumor neovascularization. *Vasc Health Risk Manag* 2005; **1**: 277–90.
7. Wouters BG, Brown JM. Cells at intermediate oxygen levels can be more important than the "hypoxic fraction" in determining tumor response to fractionated radiotherapy. *Radiat Res* 1997; **147**: 541–50.
8. Bocci G, Nicolaou KC, Kerbel RS. Protracted low-dose effects on human endothelial cell proliferation and survival *in vitro* reveal a selective antiangiogenic window for various chemotherapeutic drugs. *Cancer Res* 2002; **62**: 6938–43.
9. Hara T, Bansal A, DeGrado TR. Effect of hypoxia on the uptake of [methyl-3H] choline, [1-14C] acetate and [18F]FDG in cultured prostate cancer cells. *Nucl Med Biol* 2006; **33**: 977–84.
10. Marusyk A, Polyak K. Tumor heterogeneity: causes and consequences. *Biochim Biophys Acta* 2010; **1805**: 105–17. doi: 10.1016/j.bbcan.2009.11.002
11. Fidler IJ, Hart IR. Biological diversity in metastatic neoplasms: origins and implications. *Science* 1982; **217**: 998–1003.
12. Heppner GH. Tumor heterogeneity. *Cancer Res* 1984; **44**: 2259–65.
13. Van der Meeren A, Monti P, Vandamme M, Squiban C, Wysocki J, Griffiths N. Abdominal radiation exposure elicits inflammatory responses and abscopal effects in the lungs of mice. *Radiat Res* 2005; **163**: 144–52.
14. Abramyuk A, Tokalov S, Zophel K, Koch A, Szluha Lazanyi K, Gillham C, et al. Is pre-therapeutical FDG-PET/CT capable to detect high risk tumor subvolumes responsible for local failure in non-small cell lung cancer? *Radiother Oncol* 2009; **91**: 399–404. doi: 10.1016/j.radonc.2009.01.003
15. Benjamin LE, Golijanin D, Itin A, Pode D, Keshet E. Selective ablation of immature blood vessels in established human tumors follows vascular endothelial growth factor withdrawal. *J Clin Invest* 1999; **103**: 159–65.
16. Srinivasan A, Mohan S, Mukherji SK. Biologic imaging of head and neck cancer: the present and the future. *AJNR Am J Neuroradiol* 2012; **33**: 586–94. doi: 10.3174/ajnr.A2535
17. Miles KA, Charnsangavej C, Lee FT, Fishman EK, Horton K, Lee TY. Application of CT in the investigation of angiogenesis in oncology. *Acad Radiol* 2000; **7**: 840–50.
18. Abramyuk A, Wolf G, Shakirin G, Haberland U, Tokalov S, Koch A, et al. Preliminary assessment of dynamic contrast-enhanced CT implementation in pretreatment FDG-PET/CT for outcome prediction in head and neck tumors. *Acta Radiol* 2010; **51**: 793–9. doi: 10.3109/02841851.2010.491092
19. *WHO handbook for reporting results of cancer treatment. Offset publication no. 48*. Geneva, Switzerland: World Health Organization; 1979.
20. Tofts PS, Brix G, Buckley DL, Evelhoch JL, Henderson E, Knopp MV, et al. Estimating kinetic parameters from dynamic contrast-enhanced T(1)-weighted MRI of a diffusable tracer: standardized quantities and symbols. *J Magn Reson Imaging* 1999; **10**: 223–32.
21. Patankar TF, Haroon HA, Mills SJ, Balériaux D, Buckley DL, Parker GJ, et al. Is volume transfer coefficient (K(trans)) related to histologic grade in human gliomas? *AJNR Am J Neuroradiol* 2005; **26**: 2455–65.

22. Plotnick RE, Gardner RH, Hargrove WW, Prestegaard K, Perlmutter M. Lacunarity analysis: a general technique for the analysis of spatial patterns. *Phys Rev E Stat Phys Plasmas Fluids Relat Interdiscip Topics* 1996; **53**: 5461–8.
23. Smith TG Jr, Lange GD, Marks WB. Fractal methods and results in cellular morphology —dimensions, lacunarity and multifractals. *J Neurosci Methods* 1996; **69**: 123–36.
24. Goh V, Sanghera B, Wellsted DM, Sundin J, Halligan S. Assessment of the spatial pattern of colorectal tumour perfusion estimated at perfusion CT using two-dimensional fractal analysis. *Eur Radiol* 2009; **19**: 1358–65.
25. Cao Y, Tsien CI, Sundgren PC, Nagesh V, Normolle D, Buchtel H, et al. Dynamic contrast-enhanced magnetic resonance imaging as a biomarker for prediction of radiation-induced neurocognitive dysfunction. *Clin Cancer Res* 2009; **15**: 1747–54. doi: 10.1158/1078-0432.CCR-08-1420
26. Almeida-Freitas DB, Pinho MC, Otaduy MC, Braga HF, Meira-Freitas D, da Costa Leite C. Assessment of irradiated brain metastases using dynamic contrast-enhanced magnetic resonance imaging. *Neuroradiology* 2014; **56**: 437–43. doi: 10.1007/s00234-014-1344-0
27. Lazanyi KS, Abramyuk A, Wolf G, Tokalov S, Zöphel K, Appold S, et al. Usefulness of dynamic contrast enhanced computed tomography in patients with non-small-cell lung cancer scheduled for radiation therapy. *Lung Cancer* 2010; **70**: 280–5. doi: 10.1016/j.lungcan.2010.03.004
28. Dugdale PE, Miles KA, Bunce I, Kelley BB, Leggett DA. CT measurement of perfusion and permeability within lymphoma masses and its ability to assess grade, activity, and chemotherapeutic response. *J Comput Assist Tomogr* 1999; **23**: 540–7.
29. Ng QS, Goh V, Milner J, Padhani AR, Saunders MI, Hoskin PJ. Acute tumor vascular effects following fractionated radiotherapy in human lung cancer: *in vivo* whole tumor assessment using volumetric perfusion computed tomography. *Int J Radiat Oncol Biol Phys* 2007; **67**: 417–24.
30. Surlan-Popovic K, Bisdas S, Rumboldt Z, Koh TS, Strojan P. Changes in perfusion CT of advanced squamous cell carcinoma of the head and neck treated during the course of concomitant chemoradiotherapy. *AJNR Am J Neuroradiol* 2010; **31**: 570–5. doi: 10.3174/ajnr.A1859
31. Gupta VK, Jaskowiak NT, Beckett MA, Mauceri HJ, Grunstein J, Johnson RS, et al. Vascular endothelial growth factor enhances endothelial cell survival and tumor radioresistance. *Cancer J* 2002; **8**: 47–54.
32. Koutsimpelas D, Brieger J, Kim DW, Stenzel M, Hast J, Mann WJ. Proangiogenic effects of ionizing irradiation on squamous cell carcinoma of the hypopharynx. *Auris Nasus Larynx* 2008; **35**: 369–75.
33. Yang Z, Tang LH, Klimstra DS. Effect of tumor heterogeneity on the assessment of Ki67 labeling index in well-differentiated neuroendocrine tumors metastatic to the liver: implications for prognostic stratification. *Am J Surg Pathol* 2011; **35**: 853–60. doi: 10.1097/PAS.0b013e31821a0696
34. Bisdas S, Rumboldt Z, Surlan-Popovic K, Baghi M, Koh TS, Vogl TJ, et al. Perfusion CT in squamous cell carcinoma of the upper aerodigestive tract: long-term predictive value of baseline perfusion CT measurements. *AJNR Am J Neuroradiol* 2010; **31**: 576–81. doi: 10.3174/ajnr.A1852
35. Hermans R, Meijerink M, Van den Bogaert W, Rijnders A, Weltens C, Lambin P. Tumor perfusion rate determined noninvasively by dynamic computed tomography predicts outcome in head-and-neck cancer after radiotherapy. *Int J Radiat Oncol Biol Phy* 2003; **57**: 1351–6.
36. Vaupel P. Tumor microenvironmental physiology and its implications for radiation oncology. *Semin Radiat Oncol* 2004; **14**: 198–206.
37. Dankbaar JW, Hom J, Schneider T, Cheng SC, Lau BC, van der Schaaf I, et al. Dynamic perfusion CT assessment of the blood-brain barrier permeability: first pass versus delayed acquisition. *AJNR Am J Neuroradiol* 2008; **29**: 1671–6. doi: 10.3174/ajnr.A1203
38. Bektas H, Wu TC, Kasam M, Harun N, Sitton CW, Grotta JC, et al. Increased blood-brain barrier permeability on perfusion CT might predict malignant middle cerebral artery infarction. *Stroke* 2010; **41**: 2539–44. doi: 10.1161/STROKEAHA.110.591362
39. Bartoš M, Keunen O, Jirik R, Bjerkvig R, Taxt T. Perfusion analysis of dynamic contrast enhanced magnetic resonance images using a fully continuous tissue homogeneity model with mean transit time dispersion and frequency domain estimation of the signal delay. *Biosignal* 2010; **20**: 269–74.
40. Riedel S. *Pharmacokinetic modelling for dynamic contrast-enhanced MR renography.* Bachelor thesis. Luebeck, Germany: University of Luebeck; 2012.
41. Fusco R, Sansone M, Maffei S, Raiano N, Petrillo A. Dynamic contrast-enhanced MRI in breast cancer: a comparison between distributed and compartmental tracer kinetic models. *J Biomed Graphics Comput* 2012; **2**: 23–36.
42. Allain C, Cloitre M. Characterizing the lacunarity of random and deterministic fractal sets. *Phys Rev A* 1991; **44**: 3552–8.

APPENDIX A

The modified Patlak model [in Siemens Syngo New perfusion CT (PCT)] calculates the unidirectional transendothelial transfer constant with CT enhancement values after the peak contrast enhancement has been reached and utilizes a built-in delay correction algorithm. This allows the estimation of transendothelial transfer constant during the end of the first passage of contrast but avoids erroneous elevation of transendothelial transfer constant values secondary to delayed arrival of contrast, which would occur in a standard application of the Patlak model to PCT data, at least in the setting of acute cerebral ischaemia.[37,38]

APPENDIX B

Model selection: basically, all Tofts as well as adiabatic approximation to the tissue homogeneity model (ATH) assume the contrast material (CM) concentration in the tissue C_t to be expressed as a convolution of the arterial input function with some impulse response function $H(t)$.

$$C_t = \mathrm{AIF}(t) \times H(t)$$

For ATH, $H_{\mathrm{ATH}}(t)$[39] is given by

$$H_{\mathrm{ATH}}(t) = \begin{cases} 0 & t < \tau \\ F_{\mathrm{p}} & \tau \le t < T_{\mathrm{c}} + \tau \\ F_{\mathrm{p}} E \exp\left(-EF_{\mathrm{p}}/v_{\mathrm{e}}\left(t - T_{\mathrm{c}} - \tau\right)\right) & t \ge T_{\mathrm{c}} + \tau \end{cases} \quad (1)$$

For the Tofts model, $H_{\mathrm{Tofts}}(t)$[40] is given by

$$H_{\mathrm{Tofts}}(t) = K^{\mathrm{trans}} \exp\left(-k_{\mathrm{ep}} t\right) + v_{\mathrm{p}} \delta(t) \quad (2)$$

According to Fusco et al,[41] the following relations are valid between these two models:

$$K^{\text{trans}} = EF \tag{3}$$

$$v_p = T_c F \tag{4}$$

The reliability analysis of Fusco et al showed that a separation of transfer coefficient (K^{trans}) into extraction fraction E and flow F results in estimation errors of much more than 100% (table 3 in Fusco). In their fits, the capillary transit time did not leave their starting estimate of 6 s at all. By contrast, for the Tofts model, at least K^{trans} and k_{ep} estimates showed sufficient stability (table 4 in Fusco). So, we preferred to apply the Tofts model owing to the lower number of free parameters [four if a time shift between arterial input function (AIF) and C_{tissue} is included (equivalent to τ in H_{ATH} as given above) *vs* 5 in H_{ATH}], expecting more stable parameter estimates at all. For further improvement of the stability of the fit procedure, we applied the Patlak model, which is a simplification of the Tofts model by neglecting the back diffusion of CM from the interstitial to the capillary space setting k_{ep} to zero and is included in the Siemens software. Owing to this simplification, only the first part of the bolus passage is sufficiently described correctly, giving the linear relationship between the ratio of the CM concentrations in the tissue and the feeding arteries (after appropriate shifting in time) and the "Patlak time", which is the ratio of the improper integral of AIF(t) and the AIF(t) itself:

$$\frac{C_t(t)}{\text{AIF}(t)} = K^{\text{trans}} \frac{\int_0^t \text{AIF}(\tau)d\tau}{\text{AIF}(t)} \tag{5}$$

For pixels where the fit was not successful, the software applied gives parameter values of zero. These pixels were excluded from the further evaluations.

APPENDIX C

Homogeneity parameters: lacunarity is a measure of structural heterogeneity (non-uniformity) or degree of structural variance within an object depending on neighbourhood size.[22,23] Originally, the concept of lacunarity was developed to describe a property of fractals, that is, of structures that show some self-similarity meaning that some basic shape is repeated in smaller dimensions.[42] In this article, the gliding box algorithm is used for the analysis of lacunarity. Basically, a box (in the two-dimensional case a square) of size r (edge length) is placed around a pixel of a binary image (where each pixel can have only one of two states, *e.g.* bright or dark), and the number of pixels with a certain state (*e.g.* bright) within the box are counted. The conversion of CT parameter images to binary images is described below. This count is called "mass". The box is then shifted pixel by pixel, and the mass is determined for each position. A histogram of the masses occurred is generated and normalized to a histogram sum of 1—giving a probability distribution $Q(s)$ of all observed masses s. From this distribution, the first and second moments are calculated:

$$Z(1) = \sum s \cdot Q(s, r) \tag{6}$$

$$Z(2) = \sum s^2 \cdot Q(s, r) \tag{7}$$

The lacunarity Λ then is given by:

$$\Lambda(r) = \frac{Z(2)}{Z(1)^2}$$

One can show that Λ represents something like the relative variance of the distribution of masses. In our case, it depends on the fraction of bright pixels, on the box size r and also on their spatial distribution (in the sense of even or clustered). For an ideal fractal structure of infinite size, the lacunarity should be independent of the box size. For an image with bright regions of well-defined size and spacing, lacunarity is high for box sizes much less then this size (since almost all boxes are either empty or full—resulting in a high variance of the distribution of masses). For larger box sizes, the lacunarity decreases rapidly. For regularly distributed bright spots, lacunarity will be equal to one for any box size larger than the period length of the spot distribution. So, the mean slope of $\log(\Lambda)$ as a function of $\log(r)$ is a promising measure of the fractal character of an image. In the case of perfusion-related images, noisy and/or homogeneously perfused structures should result in slopes close to zero, whereas structures with certain poorer or better perfused regions should give rise to larger negative slope values. Another parameter evaluated is the fractal dimension. It describes the complexity or space-filling capacity of a pattern. According to Goh et al,[24] we determined it as the slope of log(box count) as a function of $\log(r)$ (box count here is the number of boxes needed to cover the structure, that is, the number of boxes with a mass >0). Taking into account the limited spatial resolution of CT imaging, we had to consider box sizes that were not negligible compared with the tumour sizes. Moreover, owing to pixels where the calculation of the blood supply parameters was not successful, the number of boxes being not completely filled by the tumour ROI was not negligible as well. Leaving them out in some cases would reduce the tumour region too much. Including them with a reduced mass owing to their only partially belonging to the ROI would artificially increase the lacunarity. We dealt with that problem by switching to probabilities—we normalized the number of bright pixels to the number of pixels of the box belonging to the ROI.

APPENDIX D

Binarization: first, the images were normalized so that the median in the ROI was set to a value of 10. For each pixel, we used a box-shaped neighbourhood, from which we considered only the pixels belonging to the ROI analysed. We calculated the median of this neighbourhood including the "pixel of interest" itself and set the pixel to "bright", when the pixel value was in a range of that local median $\pm$ a certain tolerance. By visual evaluation, we found a neighbourhood size of 13×13 pixels and a range of ± 0.1 (meaning $\pm 1\%$ of the median of the ROI) optimum for a sufficient balanced number of bright and dark pixels over the K^{trans} and relative tumour blood volume ROIs for all patients.